

Review

# A Short Overview on Graphene and Graphene-Related Materials for Electrochemical Gas Sensing

Mallikarjun Madagalam <sup>1,2</sup>, Mattia Bartoli <sup>2,3,\*</sup> and Alberto Tagliaferro <sup>1,4,\*</sup>

- <sup>1</sup> Department of Applied Science and Technology, Politecnico di Torino, Duca degli Abruzzi 24, 10129 Turin, Italy; mallikarjun.madagalam@polito.it
- <sup>2</sup> National Interuniversity Consortium of Materials Science and Technology (INSTM), Via Giuseppe Giusti, 9, 50121 Florence, Italy
- <sup>3</sup> Center for Sustainable Future Technologies (CSFT), Istituto Italiano di Tecnologia (IIT), Via Livorno 60, 10144 Turin, Italy
- <sup>4</sup> Faculty of Science, OntarioTech University, Simcoe Street North, Oshawa, ON L1G 0C5, Canada
- \* Correspondence: mattia.bartoli@iit.it (M.B.); alberto.tagliaferro@polito.it (A.T.); Tel.: +39-011-090-3400 (M.B.); +39-011-090-7347 (A.T.)

**Abstract:** The development of new and high-performing electrode materials for sensing applications is one of the most intriguing and challenging research fields. There are several ways to approach this matter, but the use of nanostructured surfaces is among the most promising and highest performing. Graphene and graphene-related materials have contributed to spreading nanoscience across several fields in which the combination of morphological and electronic properties exploit their outstanding electrochemical properties. In this review, we discuss the use of graphene and graphene-like materials to produce gas sensors, highlighting the most relevant and new advancements in the field, with a particular focus on the interaction between the gases and the materials.

**Keywords:** graphene derivatives; electrochemical sensing; graphene tailoring



**Citation:** Madagalam, M.; Bartoli, M.; Tagliaferro, A. A Short Overview on Graphene and Graphene-Related Materials for Electrochemical Gas Sensing. *Materials* **2024**, *17*, 303. <https://doi.org/10.3390/ma17020303>

Academic Editor: Irina V. Antonova

Received: 6 December 2023

Revised: 5 January 2024

Accepted: 5 January 2024

Published: 7 January 2024



**Copyright:** © 2024 by the authors. Licensee MDPI, Basel, Switzerland. This article is an open access article distributed under the terms and conditions of the Creative Commons Attribution (CC BY) license (<https://creativecommons.org/licenses/by/4.0/>).

## 1. Introduction

The production of highly sensitive materials for electrochemical sensing is a matter of great relevance for analytic science. Actually, research is focusing on finding the best trade-off between the performance and the toughness of electrode materials [1]. In this field, graphene and graphene-related materials (GRMs) can play a game-changing role.

The outstanding electrical properties of graphene combined with its superior mechanical and optical properties have attracted great interest in electrochemical sensing applications due to the achievable sensitivity, rapid response times, and versatility in detecting a wide range of analytes never reached before [2]. The integration of graphene into electrochemical sensors has led to significant performance improvements in several fields of application, including environmental science [3], medical diagnostics [4] and quality control [5]. Graphene's astonishing performance is due to the improvement of electron transfer at the electrode interface by a combination of electronic and chemical features [6]. Furthermore, graphene and GRMs' high mechanical strength and flexibility further contribute to their utility in electrochemical sensing, ensuring the stability and longevity of sensors even under challenging conditions [7].

The tunability of graphene and GRMs allows their use across several types of sensors, including amperometric, potentiometric, and impedimetric ones. In amperometric sensing, the current generated by the electrochemical reaction at the electrode surface is measured and correlated with the concentration of the analyte. Graphene and GRMs contribute to sensitivity increments due to the combination of electrical conductivity and large surface area [8,9]. Potentiometric sensors measure the potential difference between a reference electrode and a working electrode, and the incorporation of graphene and GRMs enhance

the stability and selectivity of the sensor, allowing them to be used in pH sensing [10] or ion detection [11]. Impedimetric sensors exploit changes in the impedance of the electrode interface upon interaction with the target analyte, and graphene's conductivity and charge transport properties increase both the response rate and the sensitivity of impedimetric sensors [12]. Among all the possible applications, gas detection represents a critical application of GRMs in electrochemical sensing due to the great deal of attention that monitoring air quality [13] and ensuring workplace safety [14] have gained. GRM-based sensors are of particular interest due to their ability to selectively interact with specific gases that are able to induce changes in the electric signals detected [15]. This ability, together with the other outstanding properties of GRMs, is of paramount relevance for a new generation of highly sensitive tough materials for multiple gas sensing.

In this work, we report the most relevant achievements in the GRM-based electrodes field, focusing on pristine graphene, graphene oxide (GO) and reduced graphene oxide (rGO) and their tailored derivatives. We summarize the key electronic properties of graphene and GRMs and diffusely discuss their applications in gas sensing applications, focusing on CO<sub>2</sub>, CO, H<sub>2</sub>, NH<sub>3</sub>, NO<sub>x</sub>, H<sub>2</sub>S and SO<sub>2</sub>. We provide a concise and easy-to-be-exploited overview aimed to represent a reference point for researchers interested in approaching electrochemical sensing using neat and tailored graphene and GRMs in gas sensing.

## 2. Graphene and GRM Electrical Properties

In agreement with the International Union for Pure and Applied Chemistry Golden Book, graphene is defined as “a single carbon layer of the graphite structure, describing its nature by analogy to a polycyclic aromatic hydrocarbon of quasi infinite size” [16]. A pristine graphene layer is composed of a planar arrangement of carbon atoms bonded through three  $\sigma$  bonds with the p orbitals perpendicular to the  $sp^2$  plane, allowing a full delocalization of the  $\pi$  bonds [17–19]. This is the reason behind graphene's exceptional electrical properties, particularly its in-plane electron mobility. At room temperature, the electron mobility in graphene can reach up to 15,000 cm<sup>2</sup> V<sup>-1</sup>s<sup>-1</sup> [20] due to a peculiar band organization formed by two conical points in the electronic band diagram known as Dirac points, as shown in Figure 1.

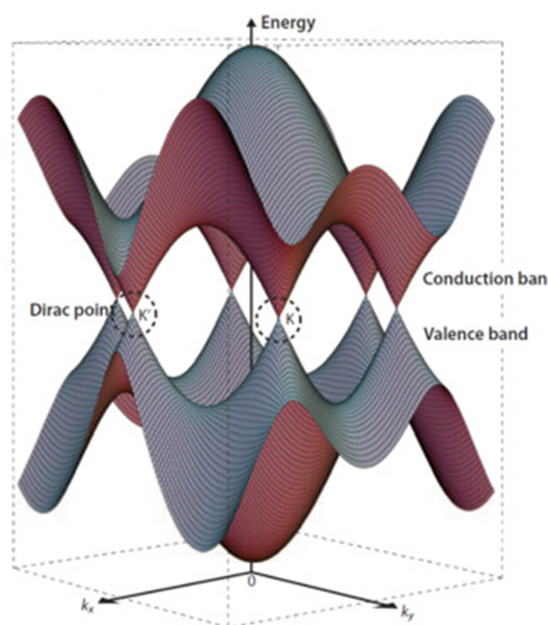


**Figure 1.** Three-dimensional schematic diagram of band structure near the Fermi level of graphene with Dirac points K and K' highlighted. Reproduced, adapted and reprinted with permission from Lavagna et al. [21].

The linear dispersion around Dirac points contributes to the massless nature of charge carriers in graphene, allowing them to travel at incredibly high speeds without any significant scattering due to the eventual topological disorder due to the temperature [22]. Furthermore, graphene is characterized by a relevant Hall effect, with the plateaus occurring at half integers of  $4 e^2/h$  rather than  $4 e^2/h$ . Near-ideal graphene sheets show a pronounced Hall effect, while multilayer samples show a much weaker gate dependence due to the electric field screening promoted by the other layers [23]. Interestingly, the use of a high magnetic field combined with cryogenic temperatures induces a quantum Hall effect for both holes and electrons [24,25]. The superb electrical properties of graphene are, however, counterbalanced by the absence of a band gap. A great effort has been devoted to creating graphene-like materials with a proper band gap [26], and solutions such as graphene nanoribbons have been developed [27]. Graphene nanoribbons can be shrunk by modifying the charge carrier momentum in the transverse direction, resulting in a band gap opening based on the ribbon width [28]. Alternatively, graphene can be doped with nanostructures and heteroatoms [29].

The most popular and useful procedure to dope graphene is oxidation with the formation of GO. GO is rich in oxygen functionalities such as epoxide and hydroxyl groups on its basal lattice, while carbonyl and carboxylic residues are more abundant on the edges, as described by the Lerf-Klinowski model [30]. The electronic properties of GO are strictly related to the degree of oxidation, as reported by Krishnamoorthy et al. [31]. The increment of GO oxidation induced a reduction of electron mobility [32] as a consequence of the introduction of more defects in the lattice structure of graphene. These defects act as scattering centers for charge carriers, hindering the smooth movement of electrons through the material. Nevertheless, the relationship between oxidation degree and electron mobility is a complex mix of factors, such as the oxygen functional groups and their distribution on the graphene lattice. Interestingly, GO shows a band gap due to the presence of the same defect that reduces the charge carrier's mobility. The oxygen functionalities alter the electronic configuration of the graphene plane, disrupting the  $\pi$ -conjugated system and forming localized states within the energy band structure of GO, giving rise to a band gap [33]. The presence of a band gap in GO promotes a semiconducting behavior contrary to pristine graphene that shows metallic conductivity [34]. This semiconducting behavior makes graphene oxide well-suited for applications in electronic devices where a controllable on/off state is essential [35]. An interesting compromise between the conductivity of pristine graphene and the properties of GO is the reduced form of GO, named rGO. rGO is produced using harsh reductive processes [36] for decreasing the oxygen residues of GO and trying to find a balance between pristine graphene and GO with a carbon/oxygen ratio ranging from 0.4 up to 13 wt% [37]. The electrical properties of rGO are far higher than those of GO but considerably inferior to graphene, while dispersibility showed an opposite trend [38].

### 3. Graphene and Graphene-Related Materials' Electrochemical Sensing Performance

Graphene and GRMs show several key features that allowed the spread of their use in electrochemical sensing applications. Firstly, GRMs are highly sensitive to the surrounding chemical and physical environment [39–41]. This is of particular interest considering the interaction with gas molecules that are adsorbed on GRMs' surface [42] that are able to alter the electronic conductivity [43]. The conductivity alteration induced by adsorbed gas prevents the correct interaction between the dangling  $\pi$ -orbitals and neighboring atom orbitals, altering the conduction bands and reducing the charge carrier's mobility. This phenomenon can be used to quantify the number of adsorbed molecules through simple electrochemical measurements in which GRMs represent the working electrode. Furthermore, the interactions between gaseous molecules and GRMs can be easily tuned by tuning the graphene functionalization, increasing both the electrochemical performance and the selectivity of the system. These features, together with a fast response and recovery

of the electrodes, have boosted the use of GRMs as electrochemical gas sensing platforms, as summarized in Table 1.

**Table 1.** Overview of the key features of graphene and GRMs in electrochemical gas sensing.

Gas	Material	Highlights	References
CO <sub>2</sub>	Chemical vapor-deposited single-layer graphene	<ul style="list-style-type: none"> <li>■ Poor responsivity.</li> <li>■ Negligible sensitivity in presence of water.</li> <li>■ Linear range up to 2000 ppm.</li> </ul>	[44]
	Exfoliated graphite nanoplatelet	<ul style="list-style-type: none"> <li>■ Good sensitivity in presence of water.</li> <li>■ Linear range 10–200 ppm.</li> </ul>	[45]
	Double-layer graphene	<ul style="list-style-type: none"> <li>■ No cross-sensitivity with H<sub>2</sub>O up to 3% relative humidity.</li> </ul>	[46]
	GO	<ul style="list-style-type: none"> <li>■ Cheap.</li> <li>■ Robust.</li> <li>■ Linear range 400–4000 ppm.</li> </ul>	[47]
	rGO	<ul style="list-style-type: none"> <li>■ Response of up to 71% in N<sub>2</sub>.</li> <li>■ Response of up to 15% in air.</li> </ul>	[48]
	Inorganics (zinc, titanium, molybdenum)-tailored graphene	<ul style="list-style-type: none"> <li>■ Operating from 10 to 60 °C.</li> <li>■ Operating up to 97% of relative humidity.</li> <li>■ Linear range 300–1100 ppm.</li> </ul>	[49]
	Palladium-tailored rGO	<ul style="list-style-type: none"> <li>■ Operating at 150 °C.</li> <li>■ Operating up to 71% of relative humidity.</li> <li>■ Linear range 200–1100 ppm.</li> </ul>	[50]
	Palladium and tin oxide-tailored rGO	<ul style="list-style-type: none"> <li>■ Slow response rate of 70 s.</li> <li>■ Operating up to 85% of relative humidity due to the formation of surface channels.</li> <li>■ Linear range up to 400 ppm.</li> </ul>	[51]
	Zinc oxide-tailored rGO	<ul style="list-style-type: none"> <li>■ Fast response up to 9 s.</li> <li>■ Response of up to 82%.</li> <li>■ Recovery time of 14 s.</li> <li>■ Linear range 1–1000 ppm.</li> </ul>	[52]
	Manganese oxide-tailored rGO	<ul style="list-style-type: none"> <li>■ Fast response up to 3 s.</li> <li>■ Response up to 70 s.</li> <li>■ Linear range 1–1000 ppm.</li> </ul>	[53]
CO	Tin oxide-tailored rGO	<ul style="list-style-type: none"> <li>■ Good selectivity over ammonia, hydrogen, and water at 25 °C.</li> </ul>	[54]
	Nickel manganate rod-tailored rGO	<ul style="list-style-type: none"> <li>■ Ultra-low detection limit (0.6–1 ppm).</li> <li>■ Linear range 20–250 ppm.</li> </ul>	[55]
	Copper oxide-tailored rGO	<ul style="list-style-type: none"> <li>■ Ultra-low detection limit (0.3 ppm).</li> <li>■ Slow response rate up to 76 s.</li> <li>■ Slow recovery up to 247 s.</li> </ul>	[56]
	Cobalt and iron oxide-tailored rGO	<ul style="list-style-type: none"> <li>■ Fast response up to 0.5 s.</li> <li>■ Linear range 10–40,000 ppm.</li> </ul>	[57]
	rGO	<ul style="list-style-type: none"> <li>■ Response up to 71% with 30 ppm of CO.</li> <li>■ Sensitivity 10 ppm.</li> <li>■ Recovery time of up to 30 s.</li> </ul>	[58]
	Poly(3,4-ethylenedioxythiophene)-tailored GO	<ul style="list-style-type: none"> <li>■ Recovery of up to 42 s.</li> <li>■ Linear range 20–270 ppm.</li> </ul>	[59,60]
	Poly(N-methyl pyrrole)-tailored rGO	<ul style="list-style-type: none"> <li>■ Recovery of up to 36 s.</li> <li>■ Detection limit of 1 ppm.</li> <li>■ Linear range 10–275 ppm.</li> </ul>	[61]
	Metal organic framework-tailored rGO	<ul style="list-style-type: none"> <li>■ Fast response up to 30 s.</li> <li>■ Fast recovery up to 70 s.</li> <li>■ Great durability in CO atmosphere for over 30 days.</li> <li>■ Sensitivity of 25 ppm.</li> </ul>	[62]

Table 1. Cont.

Gas	Material	Highlights	References
H <sub>2</sub>	Palladium nanoparticles onto single-layer graphene	<ul style="list-style-type: none"> <li>Response of 33% in 1000 ppm of at H<sub>2</sub> 25 °C.</li> <li>Sensitivity of 20 ppm.</li> </ul>	[63]
	Palladium nanoparticles onto 3D-GRMs	<ul style="list-style-type: none"> <li>Response of 41.9% under 3% H<sub>2</sub> at 25 °C.</li> <li>Easy to produce.</li> </ul>	[64]
	Platinum nanoparticle-decorated rGO	<ul style="list-style-type: none"> <li>Response of 8% under 0.5% H<sub>2</sub> at 50 °C.</li> <li>Fast recovery up to 104 s.</li> </ul>	[65]
	Platinum nanoparticles onto 3D-GRMs	<ul style="list-style-type: none"> <li>High sensitivity.</li> <li>Fast response up to 9 s.</li> <li>Fast recovery up to 10 s.</li> <li>Good linearity in the range from 1 to 100 ppm.</li> </ul>	[66]
	Tin oxide onto platinum nanoparticle-decorated rGO	<ul style="list-style-type: none"> <li>Enhanced response compared with palladium-decorated rGO.</li> <li>Enhanced sensitivity compared with palladium-decorated rGO.</li> </ul>	[67]
	Tungsten-decorated GO	<ul style="list-style-type: none"> <li>Response of 50 mV in presence of H<sub>2</sub> (100 ppm).</li> <li>Use in air atmosphere.</li> <li>Detection limit of 11 ppm.</li> </ul>	[68]
	Zinc oxide-decorated GO	<ul style="list-style-type: none"> <li>Fast response up to 114 s.</li> <li>Short recovery time up to 30 s.</li> <li>Detection limit of 4 ppm.</li> </ul>	[69]
H <sub>2</sub> O	Vertically aligned graphene arrays	<ul style="list-style-type: none"> <li>Sensitivity related to relative humidity.</li> <li>Improved performance for relative humidity over 70%.</li> </ul>	[70]
	GO	<ul style="list-style-type: none"> <li>Fastest response reported of up to 0.18 s.</li> <li>Recovery time of 0.3 s.</li> <li>Operativity from 37% up to 98% relative humidity.</li> </ul>	[71]
	Zinc oxide-tailored graphene foam	<ul style="list-style-type: none"> <li>High stability.</li> <li>High regenerability.</li> <li>Linearity from 20% up to 95% relative humidity.</li> </ul>	[72]
	Zinc oxide-tailored GO	<ul style="list-style-type: none"> <li>Response of up to 1 s.</li> <li>Linearity from 20% up to 95% relative humidity.</li> </ul>	[73]
	Silver nanoparticle-tailored GO	<ul style="list-style-type: none"> <li>Sensitivity of 26 nF/% RH.</li> <li>Linear range from 11% up to 87% relative humidity.</li> </ul>	[74]
	N-[4-morpholinecarboximidamidoyl] carboximidamidoylated GO	<ul style="list-style-type: none"> <li>Response of up 20.</li> <li>Recovery time of 2 s.</li> </ul>	[75]
	Chemical vapor-deposited graphene	<ul style="list-style-type: none"> <li>Properties related to graphene layer numbers.</li> </ul>	[76]
NH <sub>3</sub>	GO	<ul style="list-style-type: none"> <li>Properties related to graphene layer numbers.</li> <li>Linear range from 10 to 100 ppm.</li> <li>Single-layer performed better than double- and multilayer electrodes.</li> </ul>	[77]
	Fluorinated GO	<ul style="list-style-type: none"> <li>Improvement over 7% performance compared with GO.</li> </ul>	[78]
	Phosphorous-doped graphene	<ul style="list-style-type: none"> <li>Limit of detection of 69 ppb.</li> <li>Improvement over 70% of electrochemical performance compared with pristine graphene.</li> </ul>	[79]
	Aniline-tailored graphene	<ul style="list-style-type: none"> <li>Easy fabrication.</li> <li>Response of 37% in 50 ppm of NH<sub>3</sub>.</li> </ul>	[80]
	Zinc oxide on rGO	<ul style="list-style-type: none"> <li>Fast response up to 2 s.</li> <li>Fast recovery up to 13 s in 350 ppm of NH<sub>3</sub>.</li> <li>Detection limit of 10 ppm.</li> </ul>	[81]
	CuFe <sub>2</sub> O <sub>4</sub> -tailored rGO	<ul style="list-style-type: none"> <li>Fast response up to 3 s.</li> <li>Fast recovery up to 6 s.</li> <li>High selectivity (over 5 times) for NH<sub>3</sub> in presence of CH<sub>3</sub>OH, CO<sub>2</sub>, benzene.</li> <li>Limit of detection of 5 ppm.</li> </ul>	[82]

Table 1. Cont.

Gas	Material	Highlights	References
NO <sub>2</sub>	Multilayered porous graphene	<ul style="list-style-type: none"> <li>■ Selective for NO<sub>2</sub> in presence of NH<sub>3</sub>.</li> <li>■ Detection limit of 25 ppb.</li> <li>■ Response independent from relative humidity.</li> </ul>	[83]
	Silicon-doped graphene	<ul style="list-style-type: none"> <li>■ High response value of up to 22 in 50 ppm of NO<sub>2</sub>.</li> <li>■ Fast response up to 126 s.</li> <li>■ Fast recovery up to 378 s.</li> <li>■ Linear range from 18 ppb up to 300 ppm.</li> <li>■ Good selectivity.</li> </ul>	[84]
	Phosphorous-doped graphene	<ul style="list-style-type: none"> <li>■ High response value of up to 59% in 50 ppm of NO<sub>2</sub>.</li> <li>■ Detection limit 1 ppm.</li> </ul>	[85]
	Metal frameworks on rGO	<ul style="list-style-type: none"> <li>■ Detection limit 0.7 ppm.</li> <li>■ Selective for NO<sub>2</sub> in presence of NH<sub>3</sub>.</li> <li>■ Nonselective for NO<sub>2</sub> in presence of NO.</li> </ul>	[86]
	Cobalt hydroxide-tailored rGO	<ul style="list-style-type: none"> <li>■ High sensitivity of 70% exposed to 100 ppm of NO<sub>2</sub>.</li> <li>■ Detection limit of 1 ppm.</li> </ul>	[87]
	Mixed iron and cobalt oxide-tailored graphene	<ul style="list-style-type: none"> <li>■ Good response of up to 50 s.</li> <li>■ Detection limit of 1 ppm.</li> </ul>	[88]
	Copper nanoparticle-tailored graphene	<ul style="list-style-type: none"> <li>■ Great reproducibility.</li> <li>■ Detection limit of 30 ppb.</li> <li>■ Slow response.</li> </ul>	[89]
H <sub>2</sub> S	Zinc oxide onto rGO	<ul style="list-style-type: none"> <li>■ Poor selectivity in presence of NO.</li> <li>■ Detection limit of 8 ppm.</li> </ul>	[90]
	Tin oxide onto rGO	<ul style="list-style-type: none"> <li>■ Fast response in 2 s using 50 ppm of H<sub>2</sub>S.</li> <li>■ Response up to 30%.</li> <li>■ Regenerable.</li> </ul>	[91]
	Cobaltite supported on graphene nanospheres	<ul style="list-style-type: none"> <li>■ Response of 30% in presence of 50 ppm of H<sub>2</sub>S.</li> <li>■ Linear range from 1 to 70 ppm.</li> </ul>	[92]
SO <sub>2</sub>	Annealed rGO	<ul style="list-style-type: none"> <li>■ Stability over 30 days in sulphur dioxide atmosphere.</li> <li>■ Detection limit 5 ppm.</li> </ul>	[93]
	Sheets of GO	<ul style="list-style-type: none"> <li>■ Moderate response up to 65 s.</li> <li>■ Fast recovery up to 100 s.</li> <li>■ Detection limit of up to 15 ppm.</li> </ul>	[94]
	rGO	<ul style="list-style-type: none"> <li>■ Response of up to 47% in 50 ppm of SO<sub>2</sub>.</li> <li>■ Detection limit of up to 5 ppm.</li> </ul>	[95]

GRMs showed some key advantages over other 2D materials such as MXenes, mostly focused on their preparation and tailoring. The synthesis of MXenes is a complex multistage process that should operate in well-controlled conditions [96] for the production of a high-quality material, similar to the single-layer graphene process. Nevertheless, GRM production has been developed and optimized for scalability, as proven by the production of GO and rGO from a wide range of cheap feedstocks under mild conditions through robust processes [97–99]. Furthermore, the carbonaceous low-dimensional materials can exploit a wide range of reactivity, fostering an easy chemical tailoring and preserving their properties [100].

### 3.1. Pristine Graphene and GRM Sensing Performance in Electrochemical Gas Detection: CO<sub>2</sub> and CO

Monitoring the asphyxiating gases produced from combustion, such as CO<sub>2</sub> and CO, is a relevant safety issue [101]. The main issue of detecting CO<sub>2</sub> through electrochemical sensing is the interference of other species in the atmosphere, such as water, CO and oxygen. Smith et al. [44] investigated the cross-sensitivity of a capacitive CO<sub>2</sub> sensor in the presence of several residual atmospheres (Ar, H<sub>2</sub>O, N<sub>2</sub>) using a chemical vapor-deposited single-layer graphene. Particularly, the authors investigated the effect of humidity on the

sensor performance, showing the absence of sensitivity towards CO<sub>2</sub> in the presence of atmospheric-level humidity. The authors simulated through density functional theory (DFT) calculations the effect of H<sub>2</sub>O and CO<sub>2</sub>, showing that the reduction in sensitivity towards CO<sub>2</sub> was due to the electronic alteration of graphene induced by the adsorbed water molecule. The study of CO<sub>2</sub> with GRMs is of great interest for producing high-performance gas sensors, and it is affected by several key factors, such as doping, as reported in Figure 2.

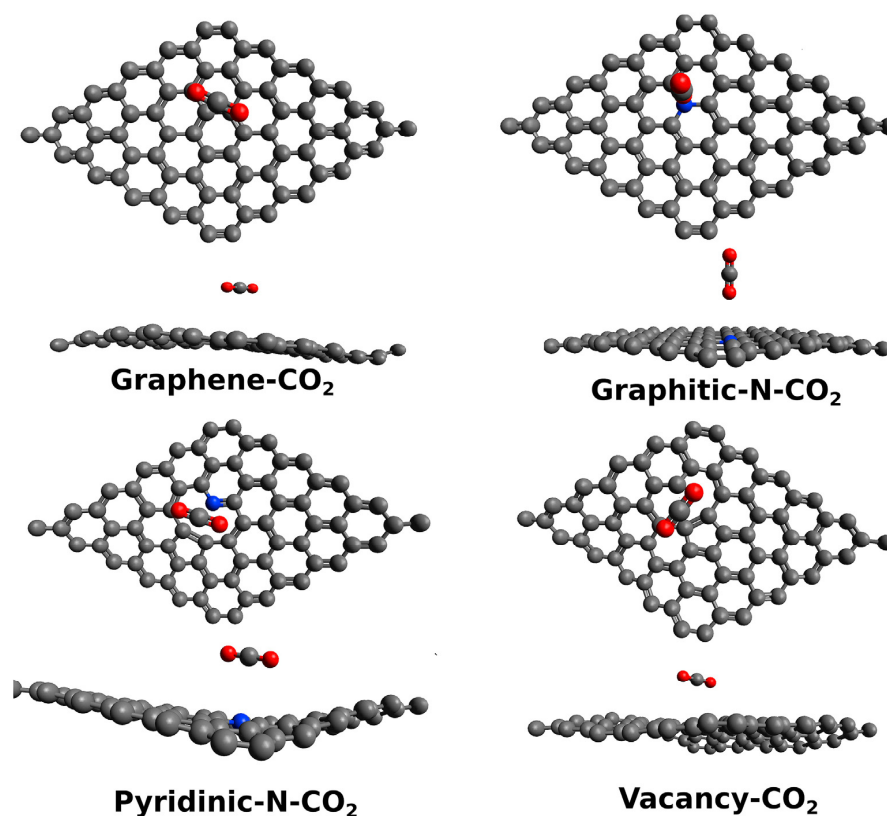


**Figure 2.** Computational simulation of the interaction between CO<sub>2</sub> and graphene or GRMs at 25 °C (carbon atoms were reported as black, oxygen atoms were reported as red and nitrogen ones as blue). Reprinted with all permission from del Castillo et al. [102].

Castillo et al. [102] investigated the role of heteroatom-doped graphene in sensing CO<sub>2</sub>, proving that the presence of nitrogen graphitic sites can alter the local morphology of graphene sheets and improving the sensitivity towards CO<sub>2</sub> over that achievable by using a Pt-decorated electrode. The authors suggested that this was due to the very same nature of nitrogen graphitic sites that act as p-type doping agents. This induced a pullout of electrons from CO<sub>2</sub>, improving the electrocatalytic activity of the nitrogen-doped graphene.

Deji et al. [103] evaluated the effect of boron and phosphorous co-doping of graphene nanoribbons for direct CO<sub>2</sub> detection using first-principle DFT simulation. The authors reported that phosphorous-doped graphene showed an adsorption energy eight times higher than pristine material, while the boron-doped one outperformed it. This study is of particular significance as it assesses the relevance of the doping agent. Additionally, Elgammal et al. [104] also proved that the support onto which graphene is deposited affects the sensing process, even if not in such a relevant way. The authors modelled the performance of graphene supported on silica or sapphire substrates for detecting both CO<sub>2</sub> and H<sub>2</sub>O molecules using DFT simulations. The results showing the differences between the substrates are in the range of 1 to 10 meV. Interestingly, authors reported that H<sub>2</sub>O molecules prefer to be adsorbed onto hollow sites in the center of the graphene hexagonal moieties, while CO<sub>2</sub> molecules prefer sites bridging carbon–carbon bonds or directly on

top of carbon atoms. Also, the authors reported that the adsorption energy of CO<sub>2</sub> was up to 0.17 eV, while H<sub>2</sub>O showed values close to 0.09 eV.

The weak interactions between CO<sub>2</sub> and graphene are a relevant issue, but several studies reported the possibility of using GRMs as solid materials for CO<sub>2</sub> sensing. Yoon et al. [45] assembled a CO<sub>2</sub> sensor fabricated by mechanical cleavage of nanographite plates. The authors were able to detect CO<sub>2</sub> at room temperature in the presence of water (humid conditions), observing a linear response of conductance in the range between 10 and 100 ppm. Fan et al. [46] used a double-layer impedimetric electrode for the detection of CO<sub>2</sub> without observing any significant influence of H<sub>2</sub>O for relative humidity (RH) up to 3%. The authors also proved that double-layer graphene performed better than single-layer due to the different spatial distribution of the electronic density.

GRMs have also been diffusely used for improving the interaction with CO<sub>2</sub>. Akhter et al. [47] designed a low-cost, low-power, miniature, highly sensitive and selective impedimetric CO<sub>2</sub> sensor using GO. The authors reported a linear range from 400 ppm to 4000 ppm with good performance in reproducibility and stability. Furthermore, they also achieved a very negligible cross-sensitivity with H<sub>2</sub>O and a fast response and recovery rate. Muhammad Hafiz et al. [48] used rGO produced by hydrogen plasma as an impedimetric sensor. The authors reported a CO<sub>2</sub> gas-sensing response of 71% (calculated as resistance variation of the electrode) in the presence of a CO<sub>2</sub> concentration up to 1500 ppm in N<sub>2</sub> and 37% RH, while the performance decreased down to a response of 15% in air environment with 68% RH. Nevertheless, the sensor showed a fast response and a good recovery rate. Alternatively, GRMs that include metal species can be used, as reported by Miao et al. [49]. The authors developed a platform system able to operate from 10 up to 60 °C with 97% RH and a CO<sub>2</sub> linear response ranging from 300 up to 1100 ppm.

CO showed a different interaction geometry with graphene, as reported by the computational study of Dindorkar et al. [105] and summarized in Figure 3.

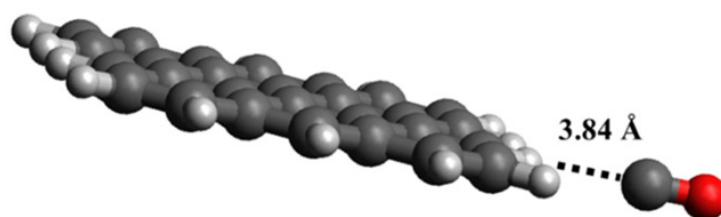


**Figure 3.** Computational simulation of the interaction between CO and graphene at 25 °C (carbon atoms were reported as black, oxygen atoms were reported as red and hydrogen ones as white). Reprinted with all permission from Dindorkar et al. [105].

While CO<sub>2</sub> preferentially interacts with carbon atoms, the CO preferential interaction is with the edges of graphene sheets (Figure 2). The authors also found that CO interacts directly with carbon atoms but only in highly doped fragments containing silicon carbide or boron nitride domains. Similar effects were reported in the presence of GO by Deji and co-workers [106] that also proved the effectiveness of the tailoring process, with metal nanoparticles decreasing the adsorption energy up to 40 times compared with pristine graphene [107]. Metal oxides combined with graphene and GRMs are able to form p-n junctions, increasing the conductivity and improving sensing performance [108]. When it comes to CO sensing, Pd has shown the most remarkable performance, as reported by Kashyap et al. [50], using palladium-tailored rGO as an impedimetric sensor. The authors tested the response to CO in the presence of both CH<sub>4</sub> and H<sub>2</sub>, suggesting that the interaction mechanism of CO was lying between the sole interactions with electron withdrawing or electron donating. As reported by Shojaee et al. [51], the combination of Pd with a metal oxide such as SnO<sub>2</sub> could be particularly beneficial for both response and recovery, improving, at the same time, the specific surface area of the material. The authors also provided an overview of the effect of RH on a 400 ppm CO sample analysis, reporting a decrement of response for RH up to 60%. They ascribed this behavior to the

competitive adsorption of CO and water molecules on the Pd and SnO<sub>2</sub>. A further RH increment of up to 85% induced a considerable increment of electrode response due to the formation of surface conductive channels [67]. The surface porosity was also investigated by Ha et al. [52] using ZnO nanoparticles onto rGO. The authors achieved an electrode response value of 85% for 1000 ppm CO at 200 °C, with a recovery time of 9 s. Similarly, the response value, response time, and recovery time of the sensor at room temperature were 27.5%, 14 s, and 15 s, respectively. The sensor demonstrated a distinct response to various CO concentrations in the range of 1–1000 ppm and good selectivity towards CO gas. In addition, the sensor exhibited good repeatability in multicycle and long-term stability. Neetha et al. [53] decorated rGO with Mn<sub>3</sub>O<sub>4</sub>, achieving a response time of only 3 s at 25 °C using 50 ppm of CO. Similar results were obtained using SnO<sub>2</sub> on graphene [54], CuO on rGO [56] and mixed metal oxide over rGO [55,57].

Nevertheless, inorganic tailoring is not a mandatory condition for detecting CO. rGO by itself can act as an active material for the detection of CO, as reported by Panda et al. [58]. The authors achieved a 71% sensitivity using 30 ppm CO at room temperature (RT), with a recovery time of up to 30 s and a remarkable sensitivity of up to 10 ppm. The authors suggested that the performance was due to the in situ production of atomic, ionic, and radical oxygen sites, which play a relevant role in both the adsorption of CO and electronic density rearmament. Furthermore, GRMs can be functionalized with polymers, as reported by Farea and co-workers [59,60] and by Mohammed et al. [61], or by metal organic frameworks boosting the overall CO sensing performance, as reported by More et al. [62].

### 3.2. Pristine Graphene and GRM Sensing Performance in Electrochemical Gas Detection: H<sub>2</sub>

H<sub>2</sub> is among the most elusive gases to be detected, and neat graphene cannot be used for direct sensing of it. The most common strategy for H<sub>2</sub> sensing is tailoring the GRM surface with metal nanoparticles, activating a mechanism known as spillover, as reported in Figure 4.

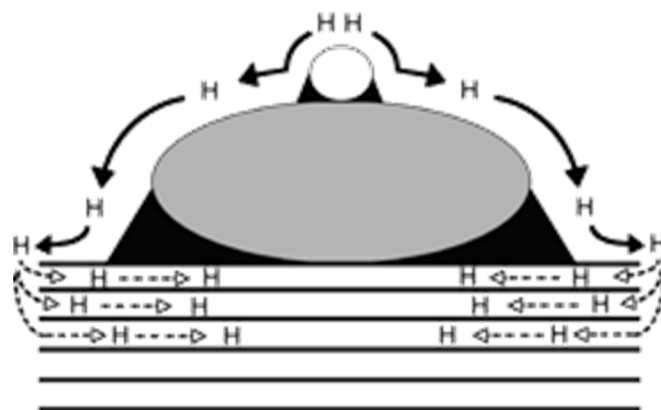


**Figure 4.** Schematic representation of primary and secondary spillover promoted by the presence of metal nanoparticles and GRMs. Reprinted with all permission from Lachawiec [109] (Copyright © 2005, American Chemical Society).

H<sub>2</sub> spillover is a complex phenomenon occurring when H<sub>2</sub> molecules dissociate onto a metal particle and diffuse as atomic hydrogen to the graphene support, while the second spillover involves a further transportation towards the carbon support. This behavior can be modulated by the introduction of layered GRMs, as reported by Kumar et al. [110], who modelled H<sub>2</sub> sensing in a GRM containing a layer of antimonene. DFT calculations showed the presence of a Bader charge transfer mechanism from the antimonene layer towards the graphene one that was able to change the potential barrier from the Ohmic to the Schottky type. Moving to tailored GRMs, Pd and Pt are the higher-performing metals due to their ability to interact with hydrogen through adsorption and release processes [111–118]. As reported by Kishnani et al. [119], palladium-doped or -decorated graphene is very effective

in sensing  $H_2$ . Particularly, the authors reported a higher electrochemical activity and conductivity for palladium-decorated graphene compared with the palladium-doped one, while the charge transfer and recovery time showed an opposite trend. Chung et al. [63] decorated a single-layer graphene sheet with palladium nanoparticles of 3 nm of average size. The authors reported a response of 33% using 1000 ppm of  $H_2$  at 25 °C and a remarkable detection limit of 20 ppm. The effect of palladium active centers was also observed by Lange et al. [120] using cyclic voltammetry without providing any highlights on the mechanism. Lee et al. [64] incorporated palladium nanoparticles into a 3D-GRM structure, reaching a response of 41.9% under 3%  $H_2$  residual atmosphere.

Platinum has also been investigated as a viable alternative to palladium. Lu et al. [65] decorated rGO with platinum nanoparticles by using freeze-drying-assisted techniques, reaching a sensitivity toward 0.5% hydrogen up to 8% and a recovery time of 63 s. Similarly, Lee et al. [64] and Phan and co-workers [66] produced a highly porous 3D-GRM containing platinum nanoparticles, achieving good linearity from 1 to 100 ppm. As reported by Russo et al. [67], the addition of  $SnO_2$  to palladium-decorated rGO was particularly beneficial, enhancing the response of palladium-decorated GRMs over four times. The authors suggested that the enhancement of sensing performance was due to the formation of a heterojunction between the n-type  $SnO_2$  and the p-type rGO in the heterostructure, boosting the catalytic effect of platinum in promoting the dissociation of  $H_2$ .

Non-noble metal oxides have also been used extensively coupled with GRMs for  $H_2$  detection. Ahmad Fauzi et al. [68] decorated a proton-conducting GO membrane with  $WO_3$ , producing a potentiometric  $H_2$  sensor. The authors claimed a response of 50 mV in the presence of  $H_2$  100 ppm in air atmosphere and a detection limit of 11 ppm.  $ZnO$  was also used with GO, with interesting results, as reported by Rasch et al. [69]. The authors achieved a very low detection limit of 4 ppm, with a very fast response of around 114 s and a small recovery time of 30 s.

### 3.3. Pristine Graphene and GRM Sensing Performance in Electrochemical Gas Detection: $H_2O$

Humidity sensors play a critical role in several industrial sectors, such as semiconductor production, in which moisture content in the air is a critical parameter [121]. GRMs provide interesting solutions to detecting the moisture content of air, even at low concentrations, due to the interaction occurring between the graphene surface and  $H_2O$  molecules, as sketched in Figure 5.

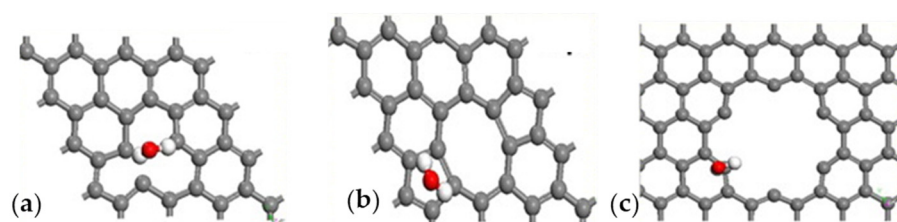


**Figure 5.** Computational simulation of the interaction between  $H_2O$  and graphene at 25 °C in (a) vacancy defect, (b) 5–7 defect and (c) close to hole defect. Reprinted with all permission from del Ye et al. [122].

As reported in Figure 3,  $H_2O$  molecules interact with graphene sheets without bonding and only through weak interactions with a distance of 2.5 Å and a higher deformation due to the interaction close to hole defects (Figure 5c), while the other cases (Figure 3a,b) did not show any significant distortion. Wang et al. [70] utilized vertically aligned graphene arrays as a humidity sensor platform. The authors observed the rise of system current with the increment of RH, suggesting a link to the Schottky barrier height with the junction resistance decrement due to the adsorption of vapor molecules. The authors suggested that the water molecules act as electron acceptors, increasing the hole density in the graphene systems. Zeng et al. [71] produced a self-powered  $H_2O$  flexible sensor with ultrafast response and recovery time of up to 0.3 s using GO. The authors claimed to have obtained a faster

response in the field of humidity sensors, and they were able to operate in an RH range from 33 to 98%. Interestingly, they proposed an interpretative model of  $H^+$  diffusion occurring during the sensing process based on Grotthuss hopping [123]. Yu et al. [121] produced a sensor based on rGO with the highest sensitivity for humidity. The authors suggested that this exceptional behavior was due to the spherical double surfaces and small pores in the 3D structure of rGO, allowing an optimal exposure of functionalities and a magnification of  $H_2O$  interactions. Nevertheless, both GO and rGO suffer several issues, such as cross-reactivity towards the other gas present in the analyte. Seeneevassen et al. [124] used a GO sensor to monitor the humidity in an effluent gas, observing that the electrode must be conditioned before use through several cycles of humidification–dehumidification.

Huang et al. [125] faced the problem of humidity quantification in the agricultural sector, in which there are many interfering agents. The authors encapsulated rGO under a layer of GO deposited by spray coating, observing a reduction in cross-sensitivity towards both  $NH_3$  and ethanol and retaining a good response and high sensitivity of up to 0.4% RH. As for the detection of other species, GRM tailoring significantly helps the sensing process, as proven by decoration with metal oxides [70,72], metal nanoparticles or organic fragments [75].

### 3.4. Pristine Graphene and GRM Sensing Performance in Electrochemical Gas Detection: $NH_3$ and $NO_x$

The detection of  $NH_3$  is highly interesting due to the harmfulness of this gas [126,127]. The interaction with graphene is also, in this case, the key to understanding how to optimize the  $NH_3$  sensing process. As shown in Figure 6 [128],  $NH_3$  interaction with graphene occurs mainly through weak hybridizations between graphene and  $NH_3$  p orbitals. Accordingly,  $NH_3$  acts as an electron donor, but pristine graphene is not able to promote both good adsorption and an efficient small transfer charge, resulting in poor detection ability.

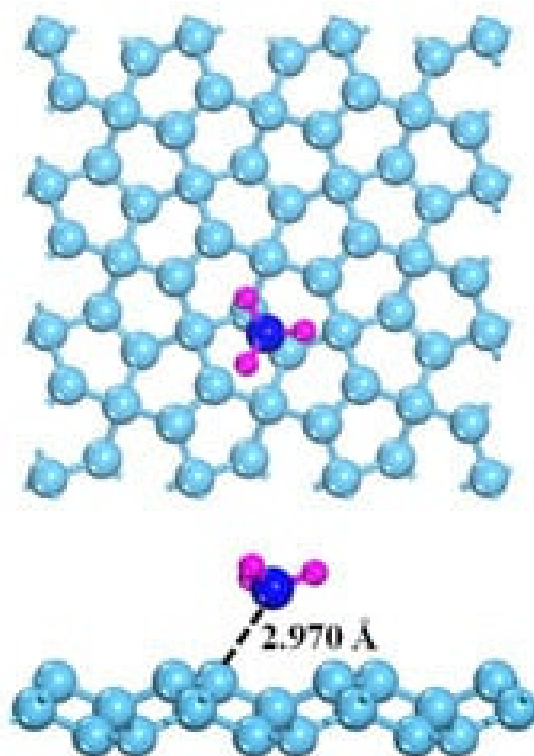


**Figure 6.** Computational simulation of the interaction between  $NH_3$  and graphene at 25 °C (carbon atoms were reported as light blue, nitrogen atoms were reported as dark blue and hydrogen ones as purple). Reprinted with all permission from Chen et al. [128].

The interaction between  $\text{NH}_3$  and graphene was evaluated by Song et al. [76]. The authors investigated the connection between sensitivity and graphene layers using single-layer, double-layer and multilayer graphene and 12,500 ppm of  $\text{NH}_3$ . The results showed that the electron transfer is three times higher in single-layer graphene than in the other species due to the easy rearrangement of charge density. Su et al. [77] used a similar approach for the production of a GO layered sensor. Also, in this case, the single-layer material showed the best performance, with a linear range from 5 to 100 ppm and a sensitivity over 15% greater than the multilayered GO. Among GRMs, fluorinated graphene also showed remarkable performance for  $\text{NH}_3$  sensing, showing a 7% change in the resistive response, while pristine GO did not show any sensing ability [78]. This behavior was due to the lower Fermi level of GO and to the increment of hole density in fluorinated GO. Alternatively, Li et al. [79] doped graphene using phosphorous for  $\text{NH}_3$  sensing. The authors reported an increment in performance with a reduction in both response and recovery time up to 71% and 73%, respectively and a detection limit of 69 ppb. Furthermore, the phosphorous-doped system showed a remarkable combination of repeatability, stability, and selectivity. The functionalization using both organic [80] and inorganic [81,82] species is also, in this case, a powerful tool for enhancing the electrochemical properties of GRMs.

$\text{NO}_x$  species represent the other great family of hazardous nitrogen-based gases [129]. Matatagui et al. [83] faced the issue represented by the detection of  $\text{NO}_2$  in the presence of  $\text{NH}_3$  using a multilayered porous graphene electrode. After photoactivation, the authors reported a change in resistance of 16% in the presence of 0.5 ppm  $\text{NO}_2$ , with a detection limit of around 25 ppb. Interestingly, the response to both  $\text{NH}_3$  (50 ppm) and  $\text{H}_2\text{O}$  (TH 33%) is negligible. The graphene decoration allowed for further improvement in the performance of the sensor by including silicon [84] or phosphorus [85], reaching a response of up to 22% and 59% resistance change using 50 ppm of  $\text{NO}_2$ .

Duy et al. [86] deeply explored the tailoring of the rGO surface with metal frameworks, including  $\text{TiO}_2$  nanoparticles and  $\text{WO}_3$ ,  $\text{WS}_2$ , and  $\text{MoS}_2$  nanoflakes using cellulose as a binder. The authors reported a sensitivity boost towards  $\text{NO}_2$ , improving the detection limit up to 0.7 ppm using  $\text{MoS}_2$  nanoflakes.  $\text{ZnO}$  oxide nanoparticles have also been diffusely used for the same scope [130–132] with poor results if compared with other nanostructures, such as cobalt supported on rGO [87], chromium-tailored graphene [133], and mixed iron and cobalt oxide [88] or copper [89] onto graphene.

### 3.5. Pristine Graphene and GRM Sensing Performance in Electrochemical Gas Detection: $\text{H}_2\text{S}$ and $\text{SO}_2$

As previously described for  $\text{NH}_3$ , the interaction between GRMs and  $\text{H}_2\text{S}$  or  $\text{SO}_2$  occurs mainly by p-orbital interactions with the  $\pi$  graphene system. As shown in Figure 7a,b,  $\text{H}_2\text{S}$  or  $\text{SO}_2$  interact with different geometry and distances due to the differences in the electron acceptor behavior of  $\text{SO}_2$ , while  $\text{H}_2\text{S}$  acts as an electron donor. Nevertheless, pristine graphene is only poorly able to detect them as a consequence of very weak interactions with them [134].

As reported in the computational research carried out by Liu et al. [87], the insertion of a dopant agent such as aluminum atoms together with Stone–Wales defects can be beneficial for boosting the adsorption of  $\text{SO}_2$ , and a similar result was reported for  $\text{H}_2\text{S}$  [135].

Ugale et al. [90] approached the detection of  $\text{H}_2\text{S}$  using  $\text{ZnO}$ -tailored rGO fibers, reaching a detection limit of 8 ppm but a poor selectivity in the presence of  $\text{NO}$ . Song et al. [91] obtained better performance using  $\text{SnO}_2$  supported on rGO, achieving a 33% response in 2 s using 50 ppm of  $\text{H}_2\text{S}$ . Furthermore, this system was totally reversible at 22 °C, allowing for long-time use. Similar results were obtained by using  $\text{Co}_3\text{O}_4$ -tailored graphene nanospheres [92] or by using copper or  $\text{WO}_3$  supported on rGO [92]. Even if the  $\text{H}_2\text{S}$  and  $\text{SO}_2$  sensing using GRMs is a field of great interest for both health and safety, the majority of the published research is currently focused more on the computational point of view rather than the applicative process, creating a perilous gap in the research [135].

It is noteworthy that Kumar et al. [93,95] deeply investigated the utilization of rGO for the detection of  $\text{SO}_2$ , achieving a limit of detection of up to 5 ppm by using annealed rGO.

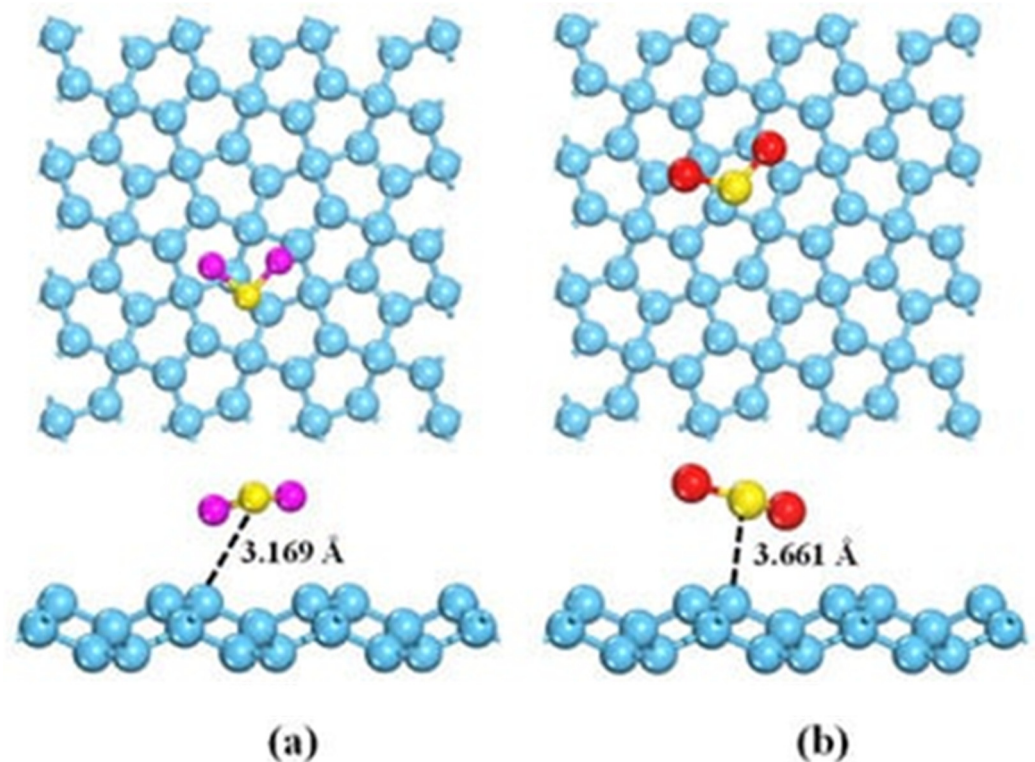


**Figure 7.** Computational simulation of the interaction between (a)  $\text{H}_2\text{S}$  and (b)  $\text{SO}_2$  and graphene at  $25^\circ\text{C}$  (carbon atoms were reported as light blue, sulphur atoms were reported as yellow, oxygen atoms were reported as red and hydrogen ones as purple). Reprinted with all permission from del Chen et al. [128].

### 3.6. Future Outlook for Pristine Graphene and GRM Gas Sensors: Wearable Devices

GRM-based gas sensors are still far from being affordable, but they show interesting perspectives for application in the production of wearable devices [136]. Wearable GRM gas sensors combine flexibility and light weight, enabling the creation of sensors integrated into clothing or into accessories and providing a non-intrusive solution for continuous gas monitoring [137,138].

This sensor family will allow for real-time monitoring, enabling continuous tracking of environmental and personal exposure to gases [139] and promoting healthcare for several activities, including those in which workers can be exposed to hazardous gases. As reported in Figure 8, Peng et al. [140] produced a humidity sensor based on laser-induced graphene that is stretchable and able to operate in real industrial environments.

The wearable GRM gas sensor has another key feature, i.e., high energy efficiency, that allows for prolonged usage without the need for frequent recharging [141]. As shown in Figure 9, Sun et al. produced a GRM-based platform able to exploit several functions, such as real-time monitoring of temperature, hydration and sweat due to the remarkable water vapor permeability.

Monitoring using high-performance electrodes will allow a significant improvement in the safety of operation in vulnerable environments such as the semiconductor and food industries, where the atmosphere should be continuously monitored, and for chemical industries operating with complex gas mixtures at high temperatures and pressures.

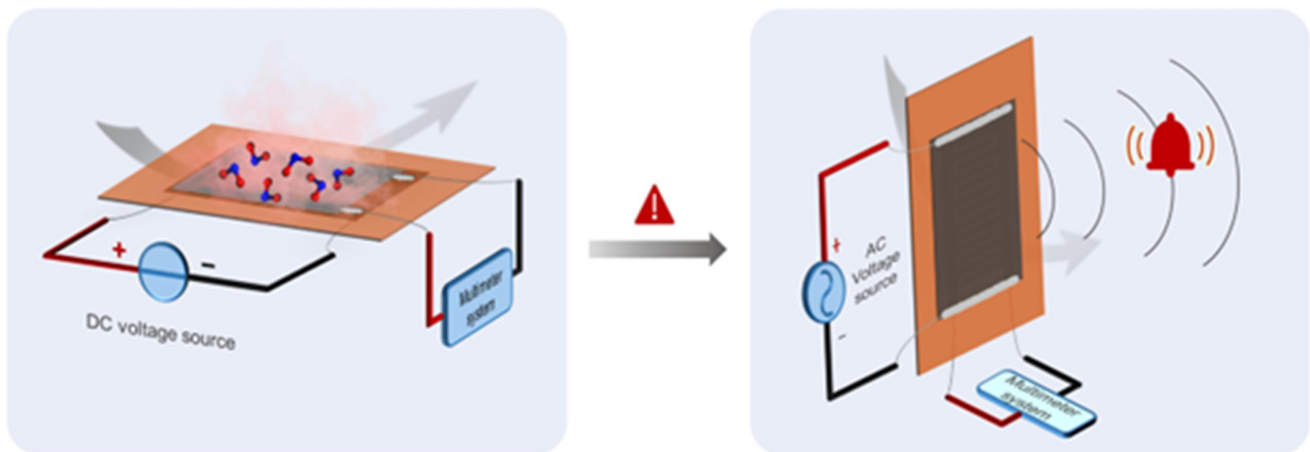


**Figure 8.** Stretchable laser-induced graphene-based humidity sensor. Reprinted with all permission from del Peng et al. [140].

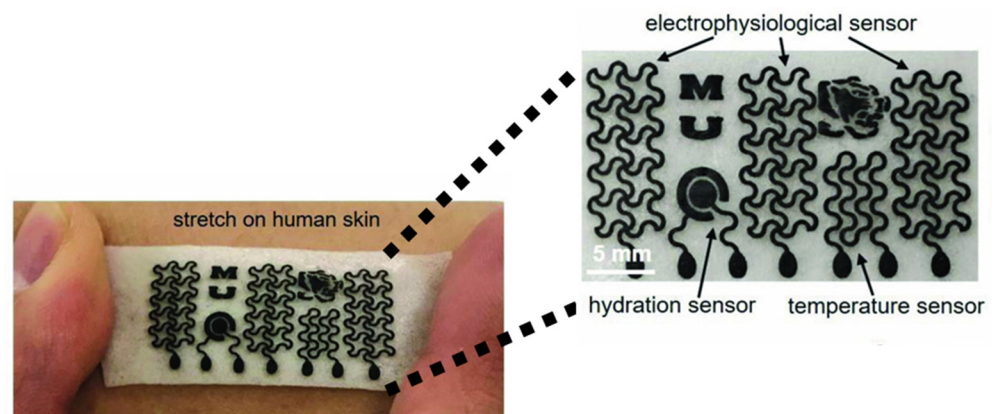


**Figure 9.** Biocompatible gas sensors based on GRM millimetric circuits. Reprinted with all permission from del Sun et al. [142].

#### 4. Conclusions

The field of gas sensors is of paramount relevance for both health and safety. The development of new high-performance materials is the key to the future of the field, and GRMs can play a relevant and active role. Nowadays, their superior performance is counterbalanced by their high cost, but a great effort has been devoted to making their industrial production more economically feasible. Nevertheless, the usage of GRM-based gas sensors can easily reach all those applications in which performance is more important than economics. Furthermore, the field of wearable gas sensors for monitoring both people's metabolism and the surrounding environment is a field of application where GRMs represent the state of the art.

We believe in the near-future scenario in which these materials will reach and improve other key sectors of daily life.

**Author Contributions:** Conceptualization, M.B. and A.T.; writing—original draft preparation, M.M. and M.B.; writing—review and editing, M.M., M.B. and A.T.; visualization, M.M. and M.B.; supervision, M.B. and A.T. All authors have read and agreed to the published version of the manuscript.

**Funding:** This research received no external funding.

**Conflicts of Interest:** The authors declare no conflicts of interest.

## References

1. Baranwal, J.; Barse, B.; Gatto, G.; Broncova, G.; Kumar, A. Electrochemical sensors and their applications: A review. *Chemosensors* **2022**, *10*, 363. [CrossRef]
2. Fu, L.; Mao, S.; Chen, F.; Zhao, S.; Su, W.; Lai, G.; Yu, A.; Lin, C.-T. Graphene-based electrochemical sensors for antibiotic detection in water, food and soil: A scientometric analysis in CiteSpace (2011–2021). *Chemosphere* **2022**, *297*, 134127. [CrossRef] [PubMed]
3. Benjamin, S.R.; Junior, E.J.M.R. Graphene based electrochemical sensors for detection of environmental pollutants. *Curr. Opin. Environ. Sci. Health* **2022**, *29*, 100381. [CrossRef]
4. Kanjwal, M.A.; Ghaferi, A.A. Graphene incorporated electrospun nanofiber for electrochemical sensing and biomedical applications: A critical review. *Sensors* **2022**, *22*, 8661. [CrossRef] [PubMed]
5. Hashim, N.; Abdullah, S.; Yusoh, K. Graphene nanomaterials in the food industries: Quality control in promising food safety to consumers. *Graphene 2D Mater.* **2022**, *7*, 1–29. [CrossRef]
6. Han, Z.; Zhang, X.; Yuan, H.; Li, Z.; Li, G.; Zhang, H.; Tan, Y. Graphene oxide/gold nanoparticle/graphite fiber microelectrodes for directing electron transfer of glucose oxidase and glucose detection. *J. Power Sources* **2022**, *521*, 230956. [CrossRef]
7. Yue, J.; Li, C.; Ji, X.; Tao, Y.; Lu, J.; Cheng, Y.; Du, J.; Wang, H. Highly tough and conductive hydrogel based on defect-patched reduction graphene oxide for high-performance self-powered flexible sensing micro-system. *Chem. Eng. J.* **2023**, *466*, 143358. [CrossRef]
8. Panraksa, Y.; Siangproh, W.; Khampieng, T.; Chailapakul, O.; Apilux, A. based amperometric sensor for determination of acetylcholinesterase using screen-printed graphene electrode. *Talanta* **2018**, *178*, 1017–1023. [CrossRef]
9. Jiang, Y.; Zhang, X.; Shan, C.; Hua, S.; Zhang, Q.; Bai, X.; Dan, L.; Niu, L. Functionalization of graphene with electrodeposited Prussian blue towards amperometric sensing application. *Talanta* **2011**, *85*, 76–81. [CrossRef]
10. Salvo, P.; Melai, B.; Calisi, N.; Paoletti, C.; Bellagambi, F.; Kirchhain, A.; Trivella, M.G.; Fuoco, R.; Di Francesco, F. Graphene-based devices for measuring pH. *Sens. Actuators B Chem.* **2018**, *256*, 976–991. [CrossRef]
11. Jaworska, E.; Lewandowski, W.; Mieczkowski, J.; Maksymiuk, K.; Michalska, A. Critical assessment of graphene as ion-to-electron transducer for all-solid-state potentiometric sensors. *Talanta* **2012**, *97*, 414–419. [CrossRef] [PubMed]
12. Bonanni, A.; Loo, A.H.; Pumera, M. Graphene for impedimetric biosensing. *TrAC Trends Anal. Chem.* **2012**, *37*, 12–21. [CrossRef]
13. Marć, M.; Tobiszewski, M.; Zabiegała, B.; de la Guardia, M.; Namieśnik, J. Current air quality analytics and monitoring: A review. *Anal. Chim. Acta* **2015**, *853*, 116–126. [CrossRef] [PubMed]
14. Pitarma, R.; Marques, G.; Ferreira, B.R. Monitoring indoor air quality for enhanced occupational health. *J. Med. Syst.* **2017**, *41*, 23. [CrossRef] [PubMed]
15. Basu, S.; Bhattacharyya, P. Recent developments on graphene and graphene oxide based solid state gas sensors. *Sens. Actuators B Chem.* **2012**, *173*, 1–21. [CrossRef]
16. International Union of Pure and Applied Chemistry (IUPAC). Graphene Layer, 3.0.1 ed. Available online: <https://goldbook.iupac.org/terms/view/G02683> (accessed on 4 January 2024).
17. Mintmire, J.W.; Dunlap, B.I.; White, C.T. Are fullerene tubules metallic? *Phys. Rev. Lett.* **1992**, *68*, 631. [CrossRef]
18. Yan, J.-A.; Ruan, W.; Chou, M. Electron-phonon interactions for optical-phonon modes in few-layer graphene: First-principles calculations. *Phys. Rev. B* **2009**, *79*, 115443. [CrossRef]
19. Dresselhaus, M.; Jorio, A.; Saito, R. Characterizing graphene, graphite, and carbon nanotubes by Raman spectroscopy. *Annu. Rev. Condens. Matter Phys.* **2010**, *1*, 89–108. [CrossRef]
20. Liu, C.-C.; Walters, A.B.; Vannice, M.A. Measurement of electrical properties of a carbon black. *Carbon* **1995**, *33*, 1699–1708. [CrossRef]
21. Lavagna, L.; Meligrana, G.; Gerbaldi, C.; Tagliaferro, A.; Bartoli, M. Graphene and Lithium-Based Battery Electrodes: A Review of Recent Literature. *Energies* **2020**, *13*, 4867. [CrossRef]
22. Siegel, D.A.; Regan, W.; Fedorov, A.V.; Zettl, A.; Lanzara, A. Charge-carrier screening in single-layer graphene. *Phys. Rev. Lett.* **2013**, *110*, 146802. [CrossRef] [PubMed]
23. Jiang, Z.; Zhang, Y.; Tan, Y.-W.; Stormer, H.; Kim, P. Quantum Hall effect in graphene. *Solid State Commun.* **2007**, *143*, 14–19. [CrossRef]
24. Xu, Z.; Zheng, Q.-S.; Chen, G. Elementary building blocks of graphene-nanoribbon-based electronic devices. *Appl. Phys. Lett.* **2007**, *90*, 223115. [CrossRef]
25. Neto, A.C.; Guinea, F.; Peres, N.M.; Novoselov, K.S.; Geim, A.K. The electronic properties of graphene. *Rev. Mod. Phys.* **2009**, *81*, 109. [CrossRef]
26. Jariwala, D.; Srivastava, A.; Ajayan, P.M. Graphene synthesis and band gap opening. *J. Nanosci. Nanotechnol.* **2011**, *11*, 6621–6641. [CrossRef] [PubMed]
27. Han, M.Y.; Özyilmaz, B.; Zhang, Y.; Kim, P. Energy band-gap engineering of graphene nanoribbons. *Phys. Rev. Lett.* **2007**, *98*, 206805. [CrossRef]
28. Li, X.; Wang, X.L.; Zhang, L.; Lee, S.; Dai, H. Chemically Derived, Ultrasoft Graphene Nanoribbon Semiconductors. *Science* **2008**, *319*, 1229. [CrossRef]
29. Rani, P.; Jindal, V. Designing band gap of graphene by B and N dopant atoms. *RSC Adv.* **2013**, *3*, 802–812. [CrossRef]
30. Lerf, A.; He, H.; Forster, M.; Klinowski, J. Structure of graphite oxide revisited. *J. Phys. Chem. B* **1998**, *102*, 4477–4482. [CrossRef]

31. Krishnamoorthy, K.; Veerapandian, M.; Yun, K.; Kim, S.-J. The chemical and structural analysis of graphene oxide with different degrees of oxidation. *Carbon* **2013**, *53*, 38–49. [[CrossRef](#)]
32. Zhu, Y.; Murali, S.; Cai, W.; Li, X.; Suk, J.W.; Potts, J.R.; Ruoff, R.S. Graphene and graphene oxide: Synthesis, properties, and applications. *Adv. Mater.* **2010**, *22*, 3906–3924. [[CrossRef](#)] [[PubMed](#)]
33. Hunt, A.; Kurmaev, E.; Moewes, A. Band gap engineering of graphene oxide by chemical modification. *Carbon* **2014**, *75*, 366–371. [[CrossRef](#)]
34. Hernández Rosas, J.; Ramírez Gutiérrez, R.; Escobedo-Morales, A.; Chigo Anota, E. First principles calculations of the electronic and chemical properties of graphene, graphane, and graphene oxide. *J. Mol. Model.* **2011**, *17*, 1133–1139. [[CrossRef](#)] [[PubMed](#)]
35. Zhu, Y.; James, D.K.; Tour, J.M. New routes to graphene, graphene oxide and their related applications. *Adv. Mater.* **2012**, *24*, 4924–4955. [[CrossRef](#)] [[PubMed](#)]
36. Guex, L.G.; Sacchi, B.; Peuvot, K.F.; Andersson, R.L.; Pourrahimi, A.M.; Ström, V.; Farris, S.; Olsson, R.T. Experimental review: Chemical reduction of graphene oxide (GO) to reduced graphene oxide (rGO) by aqueous chemistry. *Nanoscale* **2017**, *9*, 9562–9571. [[CrossRef](#)]
37. Ahmed, A.; Singh, A.; Young, S.-J.; Gupta, V.; Singh, M.; Arya, S. Synthesis techniques and advances in sensing applications of reduced graphene oxide (rGO) composites: A review. *Compos. Part A Appl. Sci. Manuf.* **2022**, *165*, 107373. [[CrossRef](#)]
38. Wang, Y.; Chen, Y.; Lacey, S.D.; Xu, L.; Xie, H.; Li, T.; Danner, V.A.; Hu, L. Reduced graphene oxide film with record-high conductivity and mobility. *Mater. Today* **2018**, *21*, 186–192. [[CrossRef](#)]
39. Mouhat, F.; Coudert, F.-X.; Bocquet, M.-L. Structure and chemistry of graphene oxide in liquid water from first principles. *Nat. Commun.* **2020**, *11*, 1566. [[CrossRef](#)]
40. Zhao, G.; Li, X.; Huang, M.; Zhen, Z.; Zhong, Y.; Chen, Q.; Zhao, X.; He, Y.; Hu, R.; Yang, T. The physics and chemistry of graphene-on-surfaces. *Chem. Soc. Rev.* **2017**, *46*, 4417–4449. [[CrossRef](#)]
41. Catania, F.; Marras, E.; Giorcelli, M.; Jagdale, P.; Lavagna, L.; Tagliaferro, A.; Bartoli, M. A Review on Recent Advancements of Graphene and Graphene-Related Materials in Biological Applications. *Appl. Sci.* **2021**, *11*, 614. [[CrossRef](#)]
42. Szcześniak, B.; Choma, J.; Jaroniec, M. Gas adsorption properties of graphene-based materials. *Adv. Colloid Interface Sci.* **2017**, *243*, 46–59. [[CrossRef](#)] [[PubMed](#)]
43. Huang, B.; Li, Z.; Liu, Z.; Zhou, G.; Hao, S.; Wu, J.; Gu, B.-L.; Duan, W. Adsorption of gas molecules on graphene nanoribbons and its implication for nanoscale molecule sensor. *J. Phys. Chem. C* **2008**, *112*, 13442–13446. [[CrossRef](#)]
44. Smith, A.D.; Elgammal, K.; Fan, X.; Lemme, M.C.; Delin, A.; Rålander, M.; Bergqvist, L.; Schröder, S.; Fischer, A.C.; Niklaus, F.; et al. Graphene-based CO<sub>2</sub> sensing and its cross-sensitivity with humidity. *RSC Adv.* **2017**, *7*, 22329–22339. [[CrossRef](#)]
45. Yoon, H.J.; Jun, D.H.; Yang, J.H.; Zhou, Z.; Yang, S.S.; Cheng, M.M.-C. Carbon dioxide gas sensor using a graphene sheet. *Sens. Actuators B Chem.* **2011**, *157*, 310–313. [[CrossRef](#)]
46. Fan, X.; Elgammal, K.; Smith, A.D.; Östling, M.; Delin, A.; Lemme, M.C.; Niklaus, F. Humidity and CO<sub>2</sub> gas sensing properties of double-layer graphene. *Carbon* **2018**, *127*, 576–587. [[CrossRef](#)]
47. Akhter, F.; Alahi, M.E.E.; Siddiquei, H.R.; Gooneratne, C.P.; Mukhopadhyay, S.C. Graphene oxide (GO) coated impedimetric gas sensor for selective detection of carbon dioxide (CO<sub>2</sub>) with temperature and humidity compensation. *IEEE Sens. J.* **2020**, *21*, 4241–4249. [[CrossRef](#)]
48. Muhammad Hafiz, S.; Ritikos, R.; Whitcher, T.J.; Razib, N.M.; Bien, D.C.S.; Chanlek, N.; Nakajima, H.; Saisopa, T.; Songsiritthigul, P.; Huang, N.M.; et al. A practical carbon dioxide gas sensor using room-temperature hydrogen plasma reduced graphene oxide. *Sens. Actuators B Chem.* **2014**, *193*, 692–700. [[CrossRef](#)]
49. Miao, F.; Han, Y.; Shi, J.; Tao, B.; Zhang, P.; Chu, P.K. Design of graphene-based multi-parameter sensors. *J. Mater. Res. Technol.* **2023**, *22*, 3156–3169. [[CrossRef](#)]
50. Kashyap, A.; Barman, P.B.; Hazra, S.K. Low-temperature selectivity study of chemically treated graphene oxide for detection of hydrogen gas. *Mater. Today Proc.* **2023**; in press. [[CrossRef](#)]
51. Shojaee, M.; Nasresfahani, S.; Sheikhi, M.H. Hydrothermally synthesized Pd-loaded SnO<sub>2</sub>/partially reduced graphene oxide nanocomposite for effective detection of carbon monoxide at room temperature. *Sens. Actuators B Chem.* **2018**, *254*, 457–467. [[CrossRef](#)]
52. Ha, N.H.; Thinh, D.D.; Huong, N.T.; Phuong, N.H.; Thach, P.D.; Hong, H.S. Fast response of carbon monoxide gas sensors using a highly porous network of ZnO nanoparticles decorated on 3D reduced graphene oxide. *Appl. Surf. Sci.* **2018**, *434*, 1048–1054. [[CrossRef](#)]
53. Neetha, J.; Abraham, K.E. Enhancement in carbon monoxide sensing performance by reduced graphene oxide/trimanganese tetraoxide system. *Sens. Actuators B Chem.* **2020**, *325*, 128749. [[CrossRef](#)]
54. Li, L.; Wang, C.; Ying, Z.; Wu, W.; Hu, Y.; Yang, W.; Xuan, W.; Li, Y.; Wen, F. SnO<sub>2</sub>/graphene nanocomposite for effective detection of CO at room temperature. *Chem. Phys. Lett.* **2023**, *830*, 140803. [[CrossRef](#)]
55. Nandi, D.; Parameswaranpillai, J.; Siengchin, S. Mechanistic insight into high response of carbon monoxide gas sensor developed by nickel manganate nanorod decorated reduced graphene oxide. *Colloids Surf. A Physicochem. Eng. Asp.* **2020**, *589*, 124449. [[CrossRef](#)]
56. Zhang, D.; Jiang, C.; Liu, J.; Cao, Y. Carbon monoxide gas sensing at room temperature using copper oxide-decorated graphene hybrid nanocomposite prepared by layer-by-layer self-assembly. *Sens. Actuators B Chem.* **2017**, *247*, 875–882. [[CrossRef](#)]

57. Zhong, Y.; Li, M.; Tan, R.; Xiao, X.; Hu, Y.; Li, G. Co(III) doped-CoFe layered double hydroxide growth with graphene oxide as cataluminescence catalyst for detection of carbon monoxide. *Sens. Actuators B Chem.* **2021**, *347*, 130600. [[CrossRef](#)]
58. Panda, D.; Nandi, A.; Datta, S.K.; Saha, H.; Majumdar, S. Selective detection of carbon monoxide (CO) gas by reduced graphene oxide (rGO) at room temperature. *RSC Adv.* **2016**, *6*, 47337–47348. [[CrossRef](#)]
59. Farea, M.A.; Mohammed, H.Y.; Shirsat, S.M.; Ali, Z.M.; Tsai, M.-L.; Yahia, I.S.; Zahran, H.Y.; Shirsat, M.D. Impact of reduced graphene oxide on the sensing performance of Poly (3, 4-ethylenedioxythiophene) towards highly sensitive and selective CO sensor: A comprehensive study. *Synth. Met.* **2022**, *291*, 117166. [[CrossRef](#)]
60. Farea, M.A.; Mohammed, H.Y.; Shirsat, S.M.; Tsai, M.-L.; Murshed, M.N.; El Sayed, M.E.; Naji, S.; Samir, A.; Alsharabi, R.M.; Shirsat, M.D. A novel approach for ultrafast and highly sensitive carbon monoxide gas sensor based on PEDOT/GO nanocomposite. *Mater. Sci. Semicond. Process.* **2023**, *155*, 107255. [[CrossRef](#)]
61. Mohammed, H.Y.; Farea, M.A.; Ali, Z.M.; Shirsat, S.M.; Tsai, M.-L.; Shirsat, M.D. Poly(N-methyl pyrrole) decorated rGO nanocomposite: A novel ultrasensitive and selective carbon monoxide sensor. *Chem. Eng. J.* **2022**, *441*, 136010. [[CrossRef](#)]
62. More, M.S.; Bodkhe, G.A.; Ingle, N.N.; Singh, F.; Tsai, M.-L.; Kim, M.; Shirsat, M.D. Metal-organic framework (MOF)/reduced graphene oxide (rGO) composite for high performance CO sensor. *Solid-State Electron.* **2023**, *204*, 108638. [[CrossRef](#)]
63. Chung, M.G.; Kim, D.-H.; Seo, D.K.; Kim, T.; Im, H.U.; Lee, H.M.; Yoo, J.-B.; Hong, S.-H.; Kang, T.J.; Kim, Y.H. Flexible hydrogen sensors using graphene with palladium nanoparticle decoration. *Sens. Actuators B Chem.* **2012**, *169*, 387–392. [[CrossRef](#)]
64. Lee, B.; Cho, S.; Jeong, B.J.; Lee, S.H.; Kim, D.; Kim, S.H.; Park, J.-H.; Yu, H.K.; Choi, J.-Y. Highly responsive hydrogen sensor based on Pd nanoparticle-decorated transfer-free 3D graphene. *Sens. Actuators B Chem.* **2024**, *401*, 134913. [[CrossRef](#)]
65. Lu, X.; Song, X.; Gu, C.; Ren, H.; Sun, Y.; Huang, J. Freeze drying-assisted synthesis of Pt@reduced graphene oxide nanocomposites as excellent hydrogen sensor. *J. Phys. Chem. Solids* **2018**, *116*, 324–330. [[CrossRef](#)]
66. Phan, D.-T.; Youn, J.-S.; Jeon, K.-J. High-sensitivity and fast-response hydrogen sensor for safety application using Pt nanoparticle-decorated 3D graphene. *Renew. Energy* **2019**, *144*, 167–171. [[CrossRef](#)]
67. Russo, P.A.; Donato, N.; Leonardi, S.G.; Baek, S.; Conte, D.E.; Neri, G.; Pinna, N. Room-temperature hydrogen sensing with heteronanostructures based on reduced graphene oxide and tin oxide. *Angew. Chem. Int. Ed.* **2012**, *51*, 11053–11057. [[CrossRef](#)] [[PubMed](#)]
68. Ahmad Fauzi, A.S.; Hamidah, N.L.; Sato, S.; Shintani, M.; Putri, G.K.; Kitamura, S.; Hatakeyama, K.; Quitain, A.T.; Kida, T. Carbon-based potentiometric hydrogen sensor using a proton conducting graphene oxide membrane coupled with a WO<sub>3</sub> sensing electrode. *Sens. Actuators B Chem.* **2020**, *323*, 128678. [[CrossRef](#)]
69. Rasch, F.; Postica, V.; Schütt, F.; Mishra, Y.K.; Nia, A.S.; Lohe, M.R.; Feng, X.; Adelung, R.; Lupan, O. Highly selective and ultra-low power consumption metal oxide based hydrogen gas sensor employing graphene oxide as molecular sieve. *Sens. Actuators B Chem.* **2020**, *320*, 128363. [[CrossRef](#)]
70. Wang, S.; Yan, H.; Zheng, H.; He, Y.; Guo, X.; Li, S.; Yang, C. Fast response humidity sensor based on chitosan/graphene oxide/tin dioxide composite. *Sens. Actuators B Chem.* **2023**, *392*, 134070. [[CrossRef](#)]
71. Zeng, S.; Pan, Q.; Huang, Z.; Gu, C.; Wang, T.; Xu, J.; Yan, Z.; Zhao, F.; Li, P.; Tu, Y.; et al. Ultrafast response of self-powered humidity sensor of flexible graphene oxide film. *Mater. Des.* **2023**, *226*, 111683. [[CrossRef](#)]
72. Morsy, M.; Ibrahim, M.; Yuan, Z.; Meng, F. Graphene Foam Decorated With ZnO as a Humidity Sensor. *IEEE Sens. J.* **2020**, *20*, 1721–1729. [[CrossRef](#)]
73. Xuan, W.; He, M.; Meng, N.; He, X.; Wang, W.; Chen, J.; Shi, T.; Hasan, T.; Xu, Z.; Xu, Y.; et al. Fast Response and High Sensitivity ZnO/glass Surface Acoustic Wave Humidity Sensors Using Graphene Oxide Sensing Layer. *Sci. Rep.* **2014**, *4*, 7206. [[CrossRef](#)] [[PubMed](#)]
74. Li, N.; Chen, X.; Chen, X.; Ding, X.; Zhao, X. Ultrahigh humidity sensitivity of graphene oxide combined with Ag nanoparticles. *Rsc Adv.* **2017**, *7*, 45988–45996. [[CrossRef](#)]
75. Shen, Q.-Q.; Zhang, C.-Z.; Bai, Y.; Ni, M.-R. Synthesizing N-[4-morpholinecarboximidamidoyl]carboximidamidoylated graphene oxide for fabricating high-sensitive humidity sensors. *Diam. Relat. Mater.* **2022**, *126*, 109053. [[CrossRef](#)]
76. Song, H.; Li, X.; Cui, P.; Guo, S.; Liu, W.; Wang, X. Sensitivity investigation for the dependence of monolayer and stacking graphene NH<sub>3</sub> gas sensor. *Diam. Relat. Mater.* **2017**, *73*, 56–61. [[CrossRef](#)]
77. Su, P.-G.; Liao, Z.-H. Fabrication of a flexible single-yarn NH<sub>3</sub> gas sensor by layer-by-layer self-assembly of graphene oxide. *Mater. Chem. Phys.* **2019**, *224*, 349–356. [[CrossRef](#)]
78. Park, M.-S.; Kim, K.H.; Kim, M.-J.; Lee, Y.-S. NH<sub>3</sub> gas sensing properties of a gas sensor based on fluorinated graphene oxide. *Colloids Surf. A Physicochem. Eng. Asp.* **2016**, *490*, 104–109. [[CrossRef](#)]
79. Li, Q.; Sun, M.; Jiang, C.; Song, S.; Li, T.; Xu, M.; Chen, W.; Peng, H. Phosphorus doping of graphene for conductometric room temperature ammonia sensing. *Sens. Actuators B Chem.* **2023**, *379*, 133234. [[CrossRef](#)]
80. Huang, X.; Hu, N.; Zhang, L.; Wei, L.; Wei, H.; Zhang, Y. The NH<sub>3</sub> sensing properties of gas sensors based on aniline reduced graphene oxide. *Synth. Met.* **2013**, *185–186*, 25–30. [[CrossRef](#)]
81. Raza, A.; Abid, R.; Murtaza, I.; Fan, T. Room temperature NH<sub>3</sub> gas sensor based on PMMA/RGO/ZnO nanocomposite films fabricated by in-situ solution polymerization. *Ceram. Int.* **2023**, *49*, 27050–27059. [[CrossRef](#)]
82. Achary, L.S.K.; Kumar, A.; Barik, B.; Nayak, P.S.; Tripathy, N.; Kar, J.P.; Dash, P. Reduced graphene oxide-CuFe<sub>2</sub>O<sub>4</sub> nanocomposite: A highly sensitive room temperature NH<sub>3</sub> gas sensor. *Sens. Actuators B Chem.* **2018**, *272*, 100–109. [[CrossRef](#)]

83. Matatagui, D.; López-Sánchez, J.; Peña, A.; Serrano, A.; del Campo, A.; de la Fuente, O.R.; Carmona, N.; Navarro, E.; Marín, P.; del Carmen Horrillo, M. Ultrasensitive NO<sub>2</sub> gas sensor with insignificant NH<sub>3</sub>-interference based on a few-layered mesoporous graphene. *Sens. Actuators B Chem.* **2021**, *335*, 129657. [[CrossRef](#)]
84. Niu, F.; Shao, Z.-W.; Gao, H.; Tao, L.-M.; Ding, Y. Si-doped graphene nanosheets for NO<sub>x</sub> gas sensing. *Sens. Actuators B Chem.* **2021**, *328*, 129005. [[CrossRef](#)]
85. Ye, X.; Qi, M.; Qiang, H.; Chen, M.; Zheng, X.; Gu, M.; Zhao, X.; Yang, Y.; He, C.; Zhang, J. Laser-ablated violet phosphorus/graphene heterojunction as ultrasensitive ppb-level room-temperature NO sensor. *Chin. Chem. Lett.* **2023**, *34*, 108199. [[CrossRef](#)]
86. Duy, L.T.; Noh, Y.G.; Seo, H. Improving graphene gas sensors via a synergistic effect of top nanocatalysts and bottom cellulose assembled using a modified filtration technique. *Sens. Actuators B Chem.* **2021**, *334*, 129676. [[CrossRef](#)]
87. Liu, S.; Zhou, L.; Yao, L.; Chai, L.; Li, L.; Zhang, G.; Kankan; Shi, K. One-pot reflux method synthesis of cobalt hydroxide nanoflake-reduced graphene oxide hybrid and their NO<sub>x</sub> gas sensors at room temperature. *J. Alloys Compd.* **2014**, *612*, 126–133. [[CrossRef](#)]
88. Zhang, C.; Zhang, S.; Zhang, D.; Yang, Y.; Zhao, J.; Yu, H.; Wang, T.; Wang, T.; Dong, X. Conductometric room temperature NO<sub>x</sub> sensor based on metal-organic framework-derived Fe<sub>2</sub>O<sub>3</sub>/Co<sub>3</sub>O<sub>4</sub> nanocomposite. *Sens. Actuators B Chem.* **2023**, *390*, 133894. [[CrossRef](#)]
89. Pungjunun, K.; Chaiyo, S.; Praphairaksit, N.; Siangproh, W.; Ortner, A.; Kalcher, K.; Chailapakul, O.; Mehmeti, E. Electrochemical detection of NO<sub>x</sub> gas based on disposable paper-based analytical device using a copper nanoparticles-modified screen-printed graphene electrode. *Biosens. Bioelectron.* **2019**, *143*, 111606. [[CrossRef](#)]
90. Ugale, A.D.; Umarji, G.G.; Jung, S.H.; Deshpande, N.G.; Lee, W.; Cho, H.K.; Yoo, J.B. ZnO decorated flexible and strong graphene fibers for sensing NO<sub>2</sub> and H<sub>2</sub>S at room temperature. *Sens. Actuators B Chem.* **2020**, *308*, 127690. [[CrossRef](#)]
91. Song, Z.; Wei, Z.; Wang, B.; Luo, Z.; Xu, S.; Zhang, W.; Yu, H.; Li, M.; Huang, Z.; Zang, J.; et al. Sensitive Room-Temperature H<sub>2</sub>S Gas Sensors Employing SnO<sub>2</sub> Quantum Wire/Reduced Graphene Oxide Nanocomposites. *Chem. Mater.* **2016**, *28*, 1205–1212. [[CrossRef](#)]
92. Liu, L.; Yang, M.; Gao, S.; Zhang, X.; Cheng, X.; Xu, Y.; Zhao, H.; Huo, L.; Major, Z. Co<sub>3</sub>O<sub>4</sub> Hollow Nanosphere-Decorated Graphene Sheets for H<sub>2</sub>S Sensing near Room Temperature. *ACS Appl. Nano Mater.* **2019**, *2*, 5409–5419. [[CrossRef](#)]
93. Kumar, R.; Kaur, A. Chemiresistive gas sensors based on thermally reduced graphene oxide for sensing sulphur dioxide at room temperature. *Diam. Relat. Mater.* **2020**, *109*, 108039. [[CrossRef](#)]
94. Van Cat, V.; Dinh, N.X.; Ngoc Phan, V.; Le, A.T.; Nam, M.H.; Dinh Lam, V.; Dang, T.V.; Quy, N.V. Realization of graphene oxide nanosheets as a potential mass-type gas sensor for detecting NO<sub>2</sub>, SO<sub>2</sub>, CO, and NH<sub>3</sub>. *Mater. Today Commun.* **2020**, *25*, 101682. [[CrossRef](#)]
95. Kumar, R.; Avasthi, D.; Kaur, A. Fabrication of chemiresistive gas sensors based on multistep reduced graphene oxide for low parts per million monitoring of sulfur dioxide at room temperature. *Sens. Actuators B Chem.* **2017**, *242*, 461–468. [[CrossRef](#)]
96. Wei, Y.; Zhang, P.; Soomro, R.A.; Zhu, Q.; Xu, B. Advances in the synthesis of 2D MXenes. *Adv. Mater.* **2021**, *33*, 2103148. [[CrossRef](#)] [[PubMed](#)]
97. Smith, A.T.; LaChance, A.M.; Zeng, S.; Liu, B.; Sun, L. Synthesis, properties, and applications of graphene oxide/reduced graphene oxide and their nanocomposites. *Nano Mater. Sci.* **2019**, *1*, 31–47. [[CrossRef](#)]
98. Alam, S.N.; Sharma, N.; Kumar, L. Synthesis of graphene oxide (GO) by modified hummers method and its thermal reduction to obtain reduced graphene oxide (rGO). *Graphene* **2017**, *6*, 1–18. [[CrossRef](#)]
99. Razaq, A.; Bibi, F.; Zheng, X.; Papadakis, R.; Jafri, S.H.M.; Li, H. Review on graphene-, graphene oxide-, reduced graphene oxide-based flexible composites: From fabrication to applications. *Materials* **2022**, *15*, 1012. [[CrossRef](#)]
100. Liu, J.; Tang, J.; Gooding, J.J. Strategies for chemical modification of graphene and applications of chemically modified graphene. *J. Mater. Chem.* **2012**, *22*, 12435–12452. [[CrossRef](#)]
101. Todorovic, A. Gases and vapours. In *Principles of Occupational Health and Hygiene*; Routledge: London, UK, 2020; pp. 242–282.
102. del Castillo, R.M.; Calles, A.G.; Espejel-Morales, R.; Hernández-Coronado, H. Adsorption of CO<sub>2</sub> on graphene surface modified with defects. *Comput. Condens. Matter* **2018**, *16*, e00315. [[CrossRef](#)]
103. Deji, Kaur, N.; Choudhary, B.C.; Sharma, R.K. Carbon-dioxide gas sensor using co-doped graphene nanoribbon: A first principle DFT study. *Mater. Today Proc.* **2021**, *45*, 5023–5028. [[CrossRef](#)]
104. Elgammal, K.; Hugosson, H.W.; Smith, A.D.; Råsander, M.; Bergqvist, L.; Delin, A. Density functional calculations of graphene-based humidity and carbon dioxide sensors: Effect of silica and sapphire substrates. *Surf. Sci.* **2017**, *663*, 23–30. [[CrossRef](#)]
105. Dindorkar, S.S.; Yadav, A. Comparative study on adsorption behaviour of the monolayer graphene, boron nitride and silicon carbide hetero-sheets towards carbon monoxide: Insights from first-principle studies. *Comput. Theor. Chem.* **2022**, *1211*, 113676. [[CrossRef](#)]
106. Deji, V.; Akarsh Kaur, N.; Choudhary, B.C.; Sharma, R.K. Adsorption chemistry of co-doped graphene nanoribbon and its derivatives towards carbon based gases for gas sensing applications: Quantum DFT investigation. *Mater. Sci. Semicond. Process.* **2022**, *146*, 106670. [[CrossRef](#)]
107. Deji, R.; Verma, A.; Kaur, N.; Choudhary, B.C.; Sharma, R.K. Density functional theory study of carbon monoxide adsorption on transition metal doped armchair graphene nanoribbon. *Mater. Today Proc.* **2022**, *54*, 771–776. [[CrossRef](#)]

108. Wang, C.; Wang, Y.; Yang, Z.; Hu, N. Review of recent progress on graphene-based composite gas sensors. *Ceram. Int.* **2021**, *47*, 16367–16384. [[CrossRef](#)]
109. Lachawiec, A.J.; Qi, G.; Yang, R.T. Hydrogen Storage in Nanostructured Carbons by Spillover: Bridge-Building Enhancement. *Langmuir* **2005**, *21*, 11418–11424. [[CrossRef](#)]
110. Kumar, N.; Jasani, J.; Sonvane, Y.; Korvink, J.G.; Sharma, A.; Sharma, B. Unfolding the hydrogen gas sensing mechanism across 2D Pnictogen/graphene heterostructure sensors. *Sens. Actuators B Chem.* **2024**, *399*, 134807. [[CrossRef](#)]
111. Frediani, M.; Oberhauser, W.; Rosi, L.; Bartoli, M.; Passaglia, E.; Capozzoli, L. Palladium nanoparticles supported onto stereocomplexed poly (lactic acid)-poly ( $\epsilon$ -caprolactone) copolymers for selective partial hydrogenation of phenylacetylene. *Rend. Lincei* **2017**, *28*, 51–58. [[CrossRef](#)]
112. Mattia Bartoli, L.R.; Petrucci, G.; Armelao, L.; Oberhauser, W.; Frediani, M.; Piccoloe, O.; Rathod, V.D.; Paganelli, S. An easily recoverable and recyclable homogeneous polyester-based Pd catalytic system for the hydrogenation of  $\alpha,\beta$ -unsaturated carbonyl compounds. *Catal. Commun.* **2015**, *69*, 228–233. [[CrossRef](#)]
113. Oberhauser, W.; Bartoli, M.; Petrucci, G.; Bandelli, D.; Frediani, M.; Capozzoli, L.; Cepek, C.; Bhardwaj, S.; Rosi, L. Nitrile hydration to amide in water: Palladium-based nanoparticles vs molecular catalyst. *J. Mol. Catal. A Chem.* **2015**, *410*, 26–33. [[CrossRef](#)]
114. Oberhauser, W.; Evangelisti, C.; Jumde, R.; Petrucci, G.; Bartoli, M.; Frediani, M.; Mannini, M.; Capozzoli, L.; Passaglia, E.; Rosi, L. Palladium-nanoparticles on end-functionalized poly(lactic acid)-based stereocomplexes for the chemoselective cinnamaldehyde hydrogenation: Effect of the end-group. *J. Catal.* **2015**, *330*, 187–196. [[CrossRef](#)]
115. Oberhauser, W.; Evangelisti, C.; Tiozzo, C.; Bartoli, M.; Frediani, M.; Passaglia, E.; Rosi, L. Platinum nanoparticles onto pegylated poly (lactic acid) stereocomplex for highly selective hydrogenation of aromatic nitrocompounds to anilines. *Appl. Catal. A Gen.* **2017**, *537*, 50–58. [[CrossRef](#)]
116. Petrucci, G.; Oberhauser, W.; Bartoli, M.; Giachi, G.; Frediani, M.; Passaglia, E.; Capozzoli, L.; Rosi, L. Pd-nanoparticles supported onto functionalized poly(lactic acid)-based stereocomplexes for partial alkyne hydrogenation. *Appl. Catal. A Gen.* **2014**, *469*, 132–138. [[CrossRef](#)]
117. Bartoli, M.; Rosi, L.; Mini, B.; Petrucci, G.; Passaglia, E.; Frediani, M. Catalytic Performances of Platinum Containing PLLA Macrocomplex in the Hydrogenation of  $\alpha, \beta$ -Unsaturated Carbonyl Compounds. *Appl. Sci.* **2019**, *9*, 3243. [[CrossRef](#)]
118. Wang, L.; Li, W.; Cai, Y.; Pan, P.; Li, J.; Bai, G.; Xu, J. Characterization of Pt-or Pd-doped graphene based on density functional theory for H<sub>2</sub> gas sensor. *Mater. Res. Express* **2019**, *6*, 095603. [[CrossRef](#)]
119. Kishnani, V.; Yadav, A.; Mondal, K.; Gupta, A. Palladium-Functionalized Graphene for Hydrogen Sensing Performance: Theoretical Studies. *Energies* **2021**, *14*, 5738. [[CrossRef](#)]
120. Lange, U.; Hirsch, T.; Mirsky, V.M.; Wolfbeis, O.S. Hydrogen sensor based on a graphene—Palladium nanocomposite. *Electrochim. Acta* **2011**, *56*, 3707–3712. [[CrossRef](#)]
121. Yu, L.; Gao, W.; R Shamshiri, R.; Tao, S.; Ren, Y.; Zhang, Y.; Su, G. Review of research progress on soil moisture sensor technology. *Int. J. Agric. Biol. Eng.* **2021**, *14*, 32–42. [[CrossRef](#)]
122. Ye, X.; Qi, M.; Yang, H.; Mediko, F.S.; Qiang, H.; Yang, Y.; He, C. Selective sensing and mechanism of patterned graphene-based sensors: Experiments and DFT calculations. *Chem. Eng. Sci.* **2022**, *247*, 117017. [[CrossRef](#)]
123. Agmon, N. The grothuss mechanism. *Chem. Phys. Lett.* **1995**, *244*, 456–462. [[CrossRef](#)]
124. Seeneevassen, S.; Leong, A.; Kashan, M.A.M.; Swamy, V.; Ramakrishnan, N. Effect of effluent gas composition on characteristics of graphene oxide film based relative humidity sensor. *Measurement* **2022**, *195*, 111156. [[CrossRef](#)]
125. Huang, Y.; Zeng, Z.; Liang, T.; Li, J.; Liao, Z.; Li, J.; Yang, T. An encapsulation strategy of graphene humidity sensor for enhanced anti-interference ability. *Sens. Actuators B Chem.* **2023**, *396*, 134517. [[CrossRef](#)]
126. Yarandi, M.S.; Mahdinia, M.; Barazandeh, J.; Soltanzadeh, A. Evaluation of the toxic effects of ammonia dispersion: Consequence analysis of ammonia leakage in an industrial slaughterhouse. *Med. Gas Res.* **2021**, *11*, 24. [[PubMed](#)]
127. Ojha, M.; Dhiman, A. Problem, failure and safety analysis of ammonia plant: A review. *Int. Rev. Chem. Eng.* **2010**, *2*, 631–646.
128. Chen, G.; Gan, L.; Xiong, H.; Zhang, H. Density Functional Theory Study of B, N, and Si Doped Penta-Graphene as the Potential Gas Sensors for NH<sub>3</sub> Detection. *Membranes* **2022**, *12*, 77. [[CrossRef](#)]
129. Choudhari, U.; Jagtap, S. A panoramic view of NO<sub>x</sub> and NH<sub>3</sub> gas sensors. *Nano-Struct. Nano-Objects* **2023**, *35*, 100995. [[CrossRef](#)]
130. Xiao, H.-M.; Hou, Y.-C.; Guo, Y.-R.; Pan, Q.-J. The coupling of graphene, graphitic carbon nitride and cellulose to fabricate zinc oxide-based sensors and their enhanced activity towards air pollutant nitrogen dioxide. *Chemosphere* **2023**, *324*, 138325. [[CrossRef](#)]
131. Ayes, A.I. The effect of ZrO<sub>x</sub> modification of graphene nanoribbon on its adsorption for NO<sub>x</sub>: A DFT investigation. *Mater. Chem. Phys.* **2022**, *291*, 126693. [[CrossRef](#)]
132. Dwivedi, G.; Deshwal, M.; Kishor Johar, A. ZnO based NO<sub>x</sub> gas and VOC detection sensor fabrication techniques and materials. *Mater. Today Proc.* **2023**. [[CrossRef](#)]
133. Wang, M.; Chen, D.; Jia, P. Adsorption and sensing performances of air decomposition components (CO, NO<sub>x</sub>) on Cr modified graphene surface. *Inorg. Chem. Commun.* **2023**, *157*, 111447. [[CrossRef](#)]
134. Reshak, A.; Auluck, S. Adsorbing H<sub>2</sub>S onto a single graphene sheet: A possible gas sensor. *J. Appl. Phys.* **2014**, *116*, 103702. [[CrossRef](#)]
135. Tan, G.-L.; Tang, D.; Wang, X.-M.; Yin, X.-T. Overview of the Recent Advancements in Graphene-Based H<sub>2</sub>S Sensors. *ACS Appl. Nano Mater.* **2022**, *5*, 12300–12319. [[CrossRef](#)]

136. Qiao, Y.; Li, X.; Hirtz, T.; Deng, G.; Wei, Y.; Li, M.; Ji, S.; Wu, Q.; Jian, J.; Wu, F. Graphene-based wearable sensors. *Nanoscale* **2019**, *11*, 18923–18945. [[CrossRef](#)] [[PubMed](#)]
137. Park, J.; Kim, J.; Kim, K.; Kim, S.-Y.; Cheong, W.H.; Park, K.; Song, J.H.; Namgoong, G.; Kim, J.J.; Heo, J.; et al. Wearable, wireless gas sensors using highly stretchable and transparent structures of nanowires and graphene. *Nanoscale* **2016**, *8*, 10591–10597.
138. Singh, E.; Meyyappan, M.; Nalwa, H.S. Flexible graphene-based wearable gas and chemical sensors. *ACS Appl. Mater. Interfaces* **2017**, *9*, 34544–34586. [[CrossRef](#)] [[PubMed](#)]
139. Xu, H.; Xiang, J.X.; Lu, Y.F.; Zhang, M.K.; Li, J.J.; Gao, B.B.; Zhao, Y.J.; Gu, Z.Z. Multifunctional wearable sensing devices based on functionalized graphene films for simultaneous monitoring of physiological signals and volatile organic compound biomarkers. *ACS Appl. Mater. Interfaces* **2018**, *10*, 11785–11793. [[CrossRef](#)]
140. Peng, Z.; Tao, L.-Q.; Zou, S.; Zhu, C.; Wang, G.; Sun, H.; Ren, T.-L. A Multi-functional NO<sub>2</sub> gas monitor and Self-Alarm based on Laser-Induced graphene. *Chem. Eng. J.* **2022**, *428*, 131079. [[CrossRef](#)]
141. Li, Q.; Wu, T.; Zhao, W.; Li, Y.; Ji, J.; Wang, G. 3D printing stretchable core-shell laser scribed graphene conductive network for self-powered wearable devices. *Compos. Part B Eng.* **2022**, *240*, 110000. [[CrossRef](#)]
142. Sun, B.; McCay, R.N.; Goswami, S.; Xu, Y.; Zhang, C.; Ling, Y.; Lin, J.; Yan, Z. Gas-Permeable, Multifunctional On-Skin Electronics Based on Laser-Induced Porous Graphene and Sugar-Templated Elastomer Sponges. *Adv. Mater.* **2018**, *30*, 1804327. [[CrossRef](#)]

**Disclaimer/Publisher’s Note:** The statements, opinions and data contained in all publications are solely those of the individual author(s) and contributor(s) and not of MDPI and/or the editor(s). MDPI and/or the editor(s) disclaim responsibility for any injury to people or property resulting from any ideas, methods, instructions or products referred to in the content.